Predictive Field-Oriented Control for Electric Drives

Fengxiang Wang[1]*, *Xuezhu Mei*[2], *Peng Tao*[1], *Ralph Kennel*[1], *and Jose Rodriguez*[3]

(1. Quanzhou Institute of Equipment Manufacturing, Haixi Institutes, Chinese Academy of Sciences, Jinjiang, 362200, China;
2. Institute for Electrical Drive Systems and Power Electronics, Technical University of Munich, Munich, 80333, Germany;
3. Faculty of Engineering, Universidad Andrés Bello, Santiago, 8370146, Chile)

Abstract: Model predictive field-oriented control (PFOC) is a novel control strategy belonging to the class of finite control set model predictive control (FCS-MPC) for electric drive systems. It is a direct control scheme which minimizes the cost function through the convergence of errors between the given and predictive stator currents. In this paper, PFOC is thoroughly presented and analyzed through its dynamics and steady state operations under wide range of speed and varying torque conditions. In light of PFOC's model based characteristics, its robustness and influence under model parameters' mismatch is also investigated. Experiments are conducted to show these performance and sensitivities.

Keywords: Model predictive control, electric drives, induction machine.

1 Introduction

The most widely applied electric drive strategy nowadays for AC motors is field-oriented control (FOC)[1]. As a linear control method, FOC requires system linearization, however, it is hard to integrate nonlinear controller with linear controllers such as PID controller. Meanwhile, with the cascaded control structure, FOC restricts the control rates of different control loops, i.e. inner current controllers' control speed must be much faster than that of the outer speed controller. This requirement on control loops also leads to limited control bandwidth, thus slower system response. Moreover, since it generates continuous voltage reference, pulse width modulation (PWM) hardware is required for voltage source inverter (VSI)'s switching state transformation. Being able to solve the above mentioned problems of FOC, model predictive control (MPC), as a kind of emerging nonlinear and direct control strategy for power electronics and electric drives[2-4], has become a research hot spot in the area.

MPC is very suitable for the control of power electronics converters because it has a discrete nature with finite number of switching states[5-6]. Similarly, a digital controller, with a sample-based manner of control, also has a discrete nature. Thus, MPC is naturally adaptable to the digital controller and requires no linearization[7]. When controlling electric drives, MPC was first presented as predictive torque control (PTC)[8-9]. PTC minimizes the error of electromagnetic torque and magnitude of the stator flux through the cost function[10]. Predictive field- oriented control (PFOC) was first proposed and applied on a VSI with RL load[11]. Because it can achieve direct nature of current control and even simpler algorithm than PTC without sacrificing performance at either steady state or transient state, it has attracted the attention of researchers and has been widely applied on various power electronics converters with both traditional and novel topologies[3,12]. However, PFOC was seldom researched for electric drives[13]. When controlling electric drives, compared to PTC, PFOC requires no weighting factor for the controlled current components in the cost function, while PTC has to pre-calculate this factor in light of the different physical attributes of controlled torque and flux quantities[14]. Thus, PFOC is theoretically much simpler than PTC for electric drives, though the research on this is in the starting phase. To unearth the PFOC's application potential in depth, this paper focuses on the analysis and experimental assessments of PFOC for electric drives. In order to discover the characters of PFOC thoroughly, experiments on a PFOC controlled induction machine with varying speed references and load torques as well as parameters' deviations are conducted[15-16], and their corresponding performance is shown and analyzed.

2 Models of voltages source inverter and induction machine

2.1 Mathematic model of inverter

A two-level three-phase VSI serves as the power converter in this work. Its topology and all feasible voltage vectors are displayed in Fig.1. Switching state $\boldsymbol{S}$ is in the form of a vector sum:

$$\boldsymbol{S}=\frac{2}{3}(S_a+\boldsymbol{a}S_b+\boldsymbol{a}^2S_c) \tag{1}$$

in which $\boldsymbol{a}=\mathrm{e}^{\mathrm{j}2\pi/3}$. $S_i,\overline{S}_i=1,0$ shows the on, off states of the upper, lower switches of lag i, with $i=a,b,c$. The output voltage vector $\boldsymbol{v}$ is of the same amplitude of DC link voltage and calculated from switching state $\boldsymbol{S}$ as:

$$\boldsymbol{v}=V_{\mathrm{dc}}\boldsymbol{S} \tag{2}$$

*Corresponding Author, E-mail: fengxiang.wang@fjirsm.ac.cn.
Supported by the National Natural Science Foundation of China under Grant 51507172.

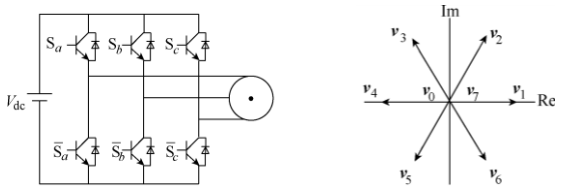

(a) VSI (b) Voltage vectors

Fig.1 Two-level three-phase VSI

2.2 Mathematic model of induction machine

A squirrel-cage IM serves as the test motor within this work. It is described by five classic electrical and mechanical equations in stationary reference frame as follows:

$$\boldsymbol{v}_{\mathrm{s}} = \boldsymbol{i}_{\mathrm{s}} \cdot R_{\mathrm{s}} + \frac{\mathrm{d}}{\mathrm{d}t}\boldsymbol{\psi}_{\mathrm{s}} \tag{3}$$

$$0 = \boldsymbol{i}_{\mathrm{r}} \cdot R_{\mathrm{r}} + \frac{\mathrm{d}}{\mathrm{d}t}\boldsymbol{\psi}_{\mathrm{r}} - \mathrm{j}\cdot\omega\cdot\boldsymbol{\psi}_{\mathrm{r}} \tag{4}$$

$$\boldsymbol{\psi}_{\mathrm{s}} = L_{\mathrm{s}} \cdot \boldsymbol{i}_{\mathrm{s}} + L_{\mathrm{m}} \cdot \boldsymbol{i}_{\mathrm{r}} \tag{5}$$

$$\boldsymbol{\psi}_{\mathrm{r}} = L_{\mathrm{r}} \cdot \boldsymbol{i}_{\mathrm{r}} + L_{\mathrm{m}} \cdot \boldsymbol{i}_{\mathrm{s}} \tag{6}$$

$$T_{\mathrm{e}} = \frac{3}{2}\cdot p \cdot Im\{\boldsymbol{\psi}_{\mathrm{s}}^{*} \cdot \boldsymbol{i}_{\mathrm{s}}\} \tag{7}$$

In the previous set of equations, $\boldsymbol{v}_{\mathrm{s}}$ is stator voltage vector. ψ_{s} and ψ_{r} represent the stator/rotor flux. $\boldsymbol{i}_{\mathrm{s}}$ and $\boldsymbol{i}_{\mathrm{r}}$ denote the stator/rotor currents. R_{s} and R_{r} are the stator/rotor resistances.

L_{s}, L_{r} and L_{m} are stator, rotor and mutual inductances. Electrical speed and pole pair number are ω and p. Electromagnetic torque is T_{e}.

3 Predictive field-oriented control

Fig.2 shows the block diagram of electric drive system with predictive field-oriented control. It is named "field-oriented control" because it requires rotor flux orientation, which is similar as the conventional field-oriented control (FOC).

3.1 Stator current prediction

Stator currents are firstly predicted with all feasible voltage vectors, and these predictions are evaluated through a cost function. The voltage vector minimizing the cost function is selected as the optimal gate signal of the IGBTs in the next sampling cycle. For long prediction steps, only the first voltage vector (corresponding to the next time step) of this optimal set is applied to the inverter referring to the receding horizon principle.

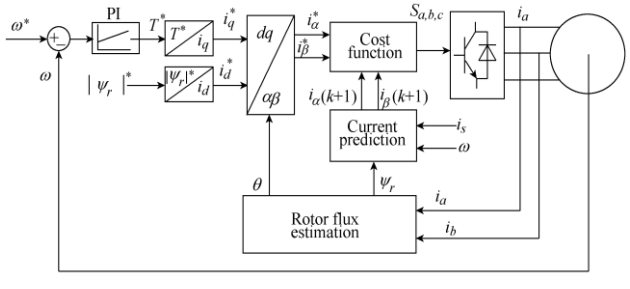

Fig.2 PFOC electric drive system

From the IM model described in section II, stator current can be further described as below:

$$\boldsymbol{i}_{\mathrm{s}} = -\frac{1}{R_{\sigma}}\left\{\left[L_{\sigma}\cdot\frac{\mathrm{d}\boldsymbol{i}_{\mathrm{s}}}{\mathrm{d}t} - k_{\mathrm{r}}\cdot\left(\frac{1}{\tau_{\mathrm{r}}} - \mathrm{j}\cdot\omega\right)\cdot\ \boldsymbol{\psi}_{\mathrm{r}}\right] - \boldsymbol{v}_{\mathrm{s}}\right\} \tag{8}$$

where $k_{\mathrm{r}} = L_{\mathrm{m}} / L_{\mathrm{r}}$, $L_{\sigma} = \sigma \cdot L_{\mathrm{s}}$ and $R_{\sigma} = R_{\mathrm{s}} + k_{\mathrm{r}}^{2} \cdot R_{\mathrm{r}}$.

First order forward Euler discretization is adopted to predict the next step's value with T_{s} as the system sampling period:

$$\frac{\mathrm{d}x}{\mathrm{d}t} \approx \frac{x(k+1) - x(k)}{T_{\mathrm{s}}} \tag{9}$$

With (8) and (9), the prediction of next step's stator current is:

$$\hat{\boldsymbol{i}}_{\mathrm{s}}(k+1) = \frac{\tau_{\sigma}}{\tau_{\sigma} + T_{\mathrm{s}}}\cdot\ \boldsymbol{i}_{\mathrm{s}}(k) + \frac{T_{\mathrm{s}}}{L_{\sigma}\left(\tau_{\sigma} + T_{\mathrm{s}}\right)}\cdot\boldsymbol{v}_{\mathrm{s}}(k) + \frac{k_{\mathrm{r}}T_{\mathrm{s}}}{\tau_{\mathrm{r}}L_{\sigma}\left(\tau_{\sigma} + T_{\mathrm{s}}\right)}\cdot\left(1 - \mathrm{j}\cdot\frac{1}{L_{\sigma}}\cdot\omega(k)\right)\cdot\ \boldsymbol{\psi}_{\mathrm{r}}(k) \tag{10}$$

where $L_{\sigma} = \sigma \cdot L_{\mathrm{s}}$ and $\tau_{\sigma} = L_{\sigma} / R_{\sigma}$.

The generation of the current references is necessary for PFOC controller. The torque reference is obtained through speed PI controller, while the rotor flux reference considered as a constant. The values of the field-producing and torque-producing current components in rotor flux reference frame are calculated as:

$$i_{\mathrm{d}}^{*} = \frac{|\boldsymbol{\psi}_{\mathrm{r}}|^{*}}{L_{\mathrm{m}}} \tag{11}$$

$$i_{\mathrm{q}}^{*} = \frac{2}{3}\frac{L_{\mathrm{r}}}{L_{\mathrm{m}}}\frac{T^{*}}{|\boldsymbol{\psi}_{\mathrm{r}}|^{*}} \tag{12}$$

The corresponding stator current vector composed with the above components is transferred into the stationary $\alpha\beta$ frame before given to the cost function.

3.2 Cost function

PFOC, as a class of FCS-MPC, contains the merit of high flexibility in cost function design and strong nonlinear control ability. Terms of control objects and system constraints can be extensively added into the cost function. The cost function in this work is expressed by the following integrated equation:

$$g_{j} = \sum_{h=2}^{N}\{|\,i_{\alpha}^{*} - i_{\alpha}(k+h)_{j}\,| + |\,i_{\beta}^{*} - i_{\beta}(k+h)_{j}\,| + \lambda\cdot\left|F_{\mathrm{s}}\left(k+1\right) - F_{\mathrm{s}}\left(k\right)\right| + \mathrm{Im}(k+h)_{j}\} \tag{13}$$

Because two-level VSI containing 7 different switching states is applied in this system, $j = 0...6$. With these 7 voltage vectors as presented in Fig.1, the cost function calculates 7 times. Thus, there are 7 possible values of g_j. The voltage vectors minimizing g_j is selected as the reference and its corresponding switching state is given to the VSI as next period's action. N is the predictive horizon. In this work, time

delay compensation is considered, thus two-steps prediction of PFOC is applied with $N=h=2$. The first two terms are the current control components of PFOC. Since they are both currents, no weighting factors are needed to be tuned between these two terms as in PTC. The third term of the cost function is the switching frequency control term that shows the switching number of the current state with the applied voltage vector. $F_s(k)$ represents the switching state for three lags of VSI. For example, if only the upper leg of the a phase is switched on, $F_s(k)$=100. λ is the weighting factor that can be tuned according to the importance of switching frequency control.

The forth term is current limitation term:

$$I_m(k+h)=\begin{cases}0 & if \quad |i(k+h)|\leqslant|i_{max}|\\ \gamma>>0 & if \quad |i(k+h)|>|i_{max}|\end{cases} \tag{14}$$

where $|i(k+h)|=\sqrt{|i_\alpha^2-i_\alpha(k+h)|+|i_\beta^2-i_\beta(k+h)|}$.

If the current is smaller than the maximum current $|i_{max}|$, the fourth term of the cost function is effective in control only when the voltage vector leads a current beyond the current limit. For the over current situation, this part increases the cost function value and thus the corresponding voltage vector is abandoned. Therewith the current limitation of the system is realized.

Based on the previous explanation, the execution of PFOC can be shown in Algorithm 1. Firstly, the rotor speed and stator currents are measured. Then the rotor flux vector is estimated. Its angle, together with the torque and flux producing currents components i_d^* and i_q^*, is used for stator current calculation in stationary frame. After that, current predictions with respect to all available voltage vectors will be made. These predictions are substituted into the cost function, and the prediction which minimizes the cost function is treated as the optimal and its corresponding voltage vector used as the applied vector for the electric drives in the next control cycle.

Algorithm 1 Execution process of PFOC strategy

Initialize the system;
Measurement of ω and i_s;
Estimation of $\boldsymbol{\psi}_r$;
Calculation of i_α^* and i_β^*;
for $j=0:6$ **do**
Prediction of $\hat{\boldsymbol{i}}_{sj}(k+1)=f(\boldsymbol{v}_{sj})$;
$g_j=\sum_{h=2}^{N}\{|i_\alpha^*-i_\alpha(k+h)_j|+|i_\beta^*-i_\beta(k+h)_j|+\lambda\cdot|F_s(k+1)-F_s(k)|+\mathrm{Im}(k+h)_j\}$
Keep the minimum value of g_j and the corresponding $\boldsymbol{v}_{sj}$;
end for
Apply $\boldsymbol{v}_{sj}$ to electric machine through VSI at next control cycle.

4 Experimental results

4.1 Motor parameters

Experiments are conducted on an IM machine with parameters in Table 1. Test bench is shown in Fig.3. The sampling frequency is set to be 16kHz.

Table 1 Induction machine parameters

Parameters	Value
DC link voltage V_{dc}/V	582
R_s/Ω	2.68
R_r/Ω	2.13
L_m/mH	275.1
L_s/mH	283.4
L_r/mH	283.4
p	1.0
ω_{nom}/(r/min)	2772.0
T_{nom}/(N·m)	7.2
J/(kg·m^2)	0.005

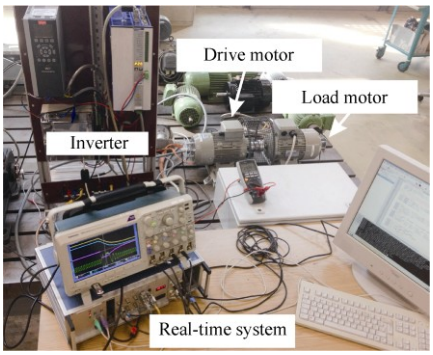

Fig.3 Test bench

4.2 Experimental results

4.2.1 Daynamic and steady states performance

In the first test, the motor operates in the full speed range. A speed reversal maneuver of rated speed from 2772r/min to –2772r/min is conducted. Fig.4 demonstrates the full speed range performance of the motor control system. The torque is set to its maximum value in the speed transition process in order to decelerate at its highest rate. Both the stator current and flux maintain their smoothness.

In the second test, a sudden torque with rated value of 7.5N·m is loaded on the motor shaft. It is seen in Fig.5 that the system can fully drag this load instantly within 50ms, while the speed is hardly reduced by this sudden load. In order to balance this torque, more power should be transferred. Thus, the magnitude of both the stator currents and stator magnetic flux are increased.

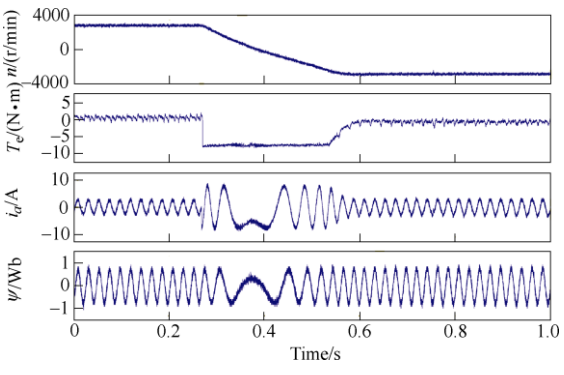

Fig.4 Behaviour under speed reversal

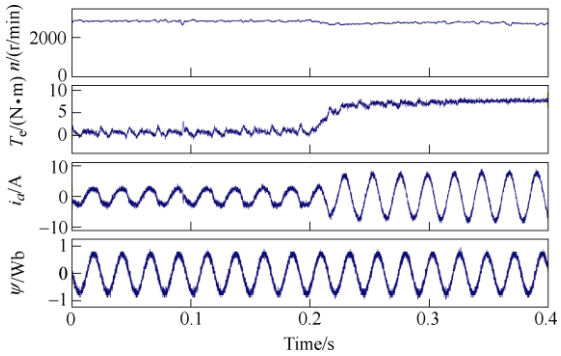

Fig.5 Behaviour under torque variation

The third test is to show the proposed PFOC electrical drive system's steady state performance. The motor is rotating at rated speed without load. From Fig.6, it is seen that in steady state, the control system has very satisfactory performance without obvious speed or torque oscillation and there is only small ripples in stators current and flux. Fig.7 observes the three phase stator currents at steady state with rated speed and torque. It proves that at the rated condition, the controlled AC motor with PCC method operates smoothly with a set of balance three phase currents. And the stator flux magnitude is kept at a constant.

4.2.2 Robustness analysis

As PFOC is model-based control, the machine model mismatches will deteriorate the control precision and dynamic performance. PFOC with longer prediction horizon control will even enlarge the cumulative error when the machine model parameters mismatches appear. Therefore, it is necessary to reveal the sensitivity and robustness of the system under parameter variation.

Firstly, the robustness against L_m variation is investigated. Since the stator flux of IM is calculated based on ratio of the measured current and L_m, the deviation of L_m causes large estimation error in flux estimation and the system may become unstable. However, compared to PTC, where both the stator and rotor fluxes estimation require L_m, in PFOC, it is only needed for stator flux estimation. Thus, PFOC should be less sensitive against L_m variation in theory. However, Fig.8 and Fig.9 show that PFOC becomes unstable with a 4% increase in L_m. Thus, it is very sensitive for L_m at both high and low speed conditions.

Electric machines, after continuous operations under loaded conditions and with the temperature

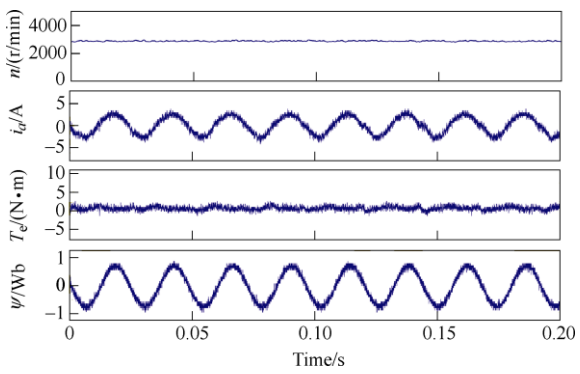

Fig.6 Steady state behaviour at rated speed without load

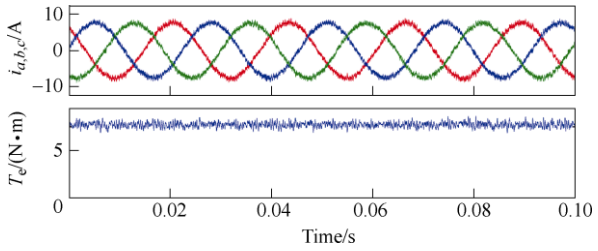

Fig.7 Steady state behaviour at rated speed with rated load

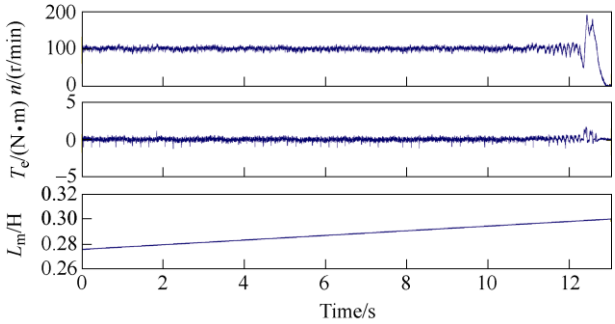

Fig.8 Sensitivity of L_m at 100r/min

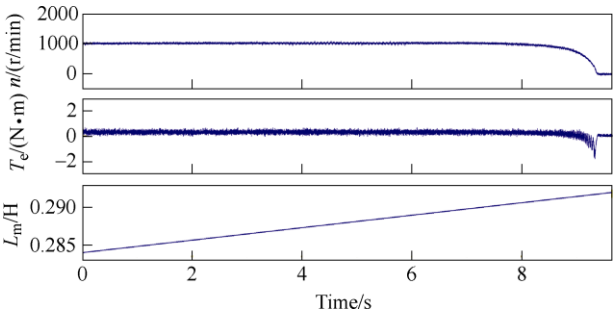

Fig.9 Sensitivity of L_m at 1000r/min

variation, will have change in resistance values. Thus, the system's robustness under resistance deviation should be studied as well.

Fig.10 shows that the system becomes unstable when the value of R_r is increased when the motor is rotating at 100 rpm, which is as expected. But when compared to the situation of L_m, system, it is much less sensitive against R_r variation. It enters the critical unstable state only when R_r is increased with 14%. As shown in Fig.11 and different from L_m, even when R_r is increased to 380% and the motor is of a speed of 1000 r/min, it is still stable without torque fluctuation.

The trend of robustness against R_s variation is similar to that of the R_r, which is shown in Fig.12 and Fig.13. The critical unstable value for R_s under 100r/min condition is with an increase of 19%.

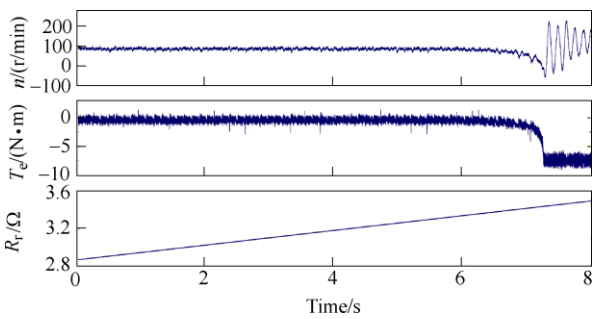

Fig.10 Sensitivity of R_r at 100r/min

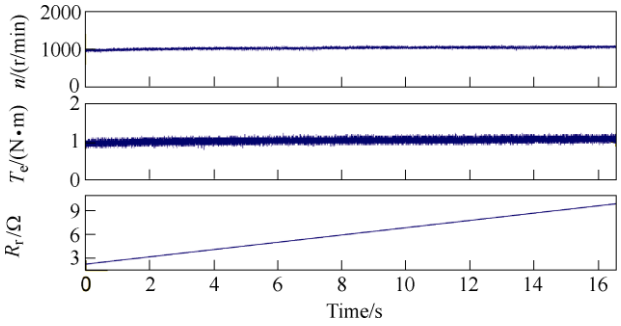

Fig.11 Sensitivity of R_r at 1000r/min

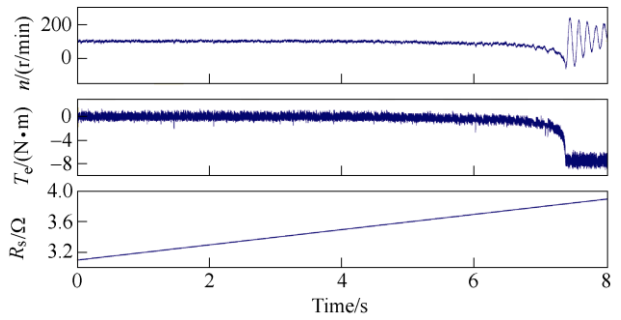

Fig.12 Sensitivity of R_s at 100r/min

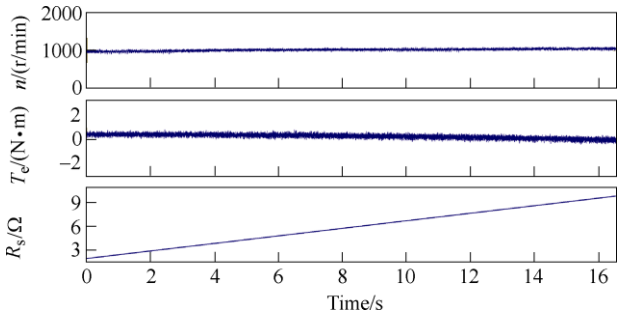

Fig.13 Sensitivity of R_s at 1000r/min

From the above results, it is found that system's robustness is closely related to the speed. For both inductance and resistances, the motor is less sensitive to their parameters' deviations when operating at middle and higher speed.

5 Conclusions

In this paper, a finite-control-set model predictive field oriented controller is proposed and applied in an induction machine control system. The experimental results show its high performance. PFOC reduces the system cost, shortens its response time and improves the general dynamics. Moreover, there is hardly any work for the cost function. These advantages are confirmed in a wide speed range at both no load and loaded conditions. PFOC controlled system's steady speed control performance, low torque ripples, ideal sinusoidal current waveform and fast response, which are essential for the low voltage drive systems. This also implies that the predicted currents can track the references very precisely. Investigations on system's robustness reveal that PFOC is sensitive to inductance deviation, and therefore a parameter observer is suggested for further improvement for implementation. At higher speed region, PFOC behaves more robustly, which verifies again a mutual character of model based controllers or estimators.

References

[1] J. Rodriguez, R. Kennel, J. Espinoza, M. Trincado, C. Silva, and C. Rojas, "High-performance control strategies for electrical drives: an experimental assessment," *IEEE Transactions on Industrial Electronics,* vol. 59, no. 2, pp. 812-20, Feb. 2012.

[2] P. Cortes, M. P. Kazmierkowski, R. M. Kennel, D. E. Quevedo, and J. Rodriguez, "Predictive control in power electronics and drives," *IEEE Transactions on Industrial Electronics*, vol. 55, no. 12, pp. 4312-4324, Dec. 2008.

[3] S. Vazquez, J. I. Leon, L. G. Franquelo, J. Rodriguez, H. A. Young, A. Marquez, and P. Zanchetta, "Model predictive control: a review of its applications in power electronics," *IEEE Industrial Electronics Magazine*, vol. 8, no. 1, pp. 16-31, March 2014.

[4] Z. Zhang, F. Wang, J. Wang, J. Rodriguez, and R. Kennel, "Nonlinear direct control for three-level npc back-to-back converter PMSG wind turbine systems: experimental assessment using FPGA," *IEEE Transactions on Industrial Informatics*, no.99, pp.1-1. DOI: 10.1109/TII.2017.2678500.

[5] C. Wang, J. Xia, and Y. Sun, *Modern Control Technology for Electric Machines*. Beijing:China Machine Press, 2014.

[6] S. Vazquez, J. Rodriguez, M. Rivera, L. G. Franquelo, and M. Norambuena, "Model predictive control for power converters and drives: advances and trends," *IEEE Transactions on Industrial Electronics*, vol. 64, no. 2, pp. 935-947, Feb. 2017.

[7] S. Kouro, M. A. Perez, J. Rodriguez, A. M. Llor,and H. A. Young, "Model predictive control: MPC's role in the evolution of power electronics," *IEEE Industrial Electronics Magazine*, vol. 9, no. 4, pp. 8-21, Dec. 2015.

[8] T. Geyer, G. Papafotiou,and M. Morari, "Model predictive direct torque control—part i: concept, algorithm, and analysis," *IEEE Transactions on Industrial Electronics*, vol. 56, no. 6, pp. 1894-1905, June 2009.

[9] F. Wang, S. A. Davari, Z. Chen, Z. Zhang, D. A. Khaburi, J. Rodriguez, and R. Kennel, "Finite control set model predictive torque control of induction machine with a robust adaptive observer," *IEEE Transactions on Industrial Electronics*, vol. 64, no. 4, pp. 2631-2641, April 2017.

[10] Y. Wang, X. Wang, W. Xie, F. Wang, M. Dou, R. M. Kennel, R. D. Lorenz,and D. Gerling, "Deadbeat model predictive torque control with discrete space vector modulation for PMSM drives," *IEEE Transactions on Industrial Electronics* , vol.64, no.5, pp.3537-3547, May 2017.

[11] J. Rodriguez, J. Pontt, C. A. Silva, P. Correa, P. Lezana, P. Cortes, and U. Ammann, "Predictive current control of a voltage source inverter," *IEEE Transactions on Industrial Electronics,* vol. 54, no. 1, pp. 495-503, Feb. 2007.

[12] A. Calle-Prado, S. Alepuz, J. Bordonau, P. Cortes, and J. Rodriguez, "Predictive control of a back-to-back NPC converter- based wind power system," *IEEE Transactions on Industrial Electronics, vol.6*3, no.7, pp. 4615-4627, July 2016.

[13] C. Garcia, J. Rodriguez, C. Silva, C. Rojas, P. Zanchetta,and H. Abu-Rub, "Full predictive cascaded speed and current control of an induction machine," *IEEE Transactions on Energy Conversion*, vol. 31, no. 3, pp. 1059-1067, Sept. 2016.

[14] P. Correa, M. Pacas,and J. Rodriguez, "Predictive torque control for inverter-fed induction machines," *IEEE Transactions on Industrial Electronics*, vol. 54, no. 2, pp. 1073-1079, Apr. 2007.

[15] M. Siami, D. A. Khaburi, A. Abbaszadeh,and J. Rodríguez, "Robustness improvement of predictive current control using prediction error correction for permanent-magnet synchronous machines," *IEEE Transactions on Industrial Electronics*, vol. 63, no. 6, pp. 3458-3466, June 2016.

[16] H. A. Young, M. A. Perez,and J. Rodriguez, "Analysis of finite-control-set model predictive current control with model parameter mismatch in a three-phase inverter," *IEEE Transactions on Industrial Electronics*, vol. 63, no. 5, pp. 3100-3107, May 2016.

Fengxiang Wang received the B.S. degree in electronic engineering and the M.S. degree in automation from Nanchang Hangkong University, Nanchang, China, in 2005 and 2008, respectively, and the Ing. (Ph.D.) degree from Technical University of Munich, Munich, Germany, in 2014. In 2014, he started working at Quanzhou Institute of Equipment Manufacturing (QIEM), Haixi Institutes, Chinese Academy of Sciences, China. He is currently a professor and the vice director of QIEM. His research interests include predictive control and sensorless control for electrical drives and power electronics.

Xuezhu Mei received the B.S. degree in electrical engineering in 2009 from Guangdong University of Technology, China and received the M. Sc. degree in electrical engineering in 2010 from University of Newcastle-upon-Tyne, UK. She is currently working toward her Ph.D. degree at the Institute for Electrical Drive Systems and Power Electronics, Technical University of Munich, Munich, Germany. Since 2014, she has become research assistant at QIEM. Her research interests include predictive control for electric drives and power electronics.

Peng Tao received the B.S. degree in 2006 from Wuhan University of Technology and the M.S. degree in 2008 from Huazhong University of Science and Technology, China. And he received the Ph.D. degree in 2014 from Chinese Academy of Sciences. He is currently a postdoctoral researcher at QIEM. His research interests include sensorless control for electrical drives and power electronics.

Ralph Kennel got his diploma degree and Dr.-Ing. degree in 1979 and1984 from the University of Kaiserslautern. From 1983 to 1999 he worked on several positions with Robert BOSCH GmbH (Germany). From 1994 to 1999 he was a visiting professor at the University of Newcastle-upon-Tyne, UK. From 1999-2008 he was professor at Wuppertal University (Germany). Since 2008 he is professor at Technical University of Munich, Germany. He is a senior member of IEEE, fellow of IEE and a chartered engineer in the UK. Within IEEE he is Treasurer of the Germany section as well as ECCE Global Partnership Chair of the Power Electronics society (PELS). His main interests are: sensorless control of AC drives, predictive control of power electronics and Hardware-in-the-Loop systems.

José Rodríguez received the Engineer degree in electrical engineering from the Universidad Federico Santa Maria, Valparaiso, Chile, in 1977 and the Dr.-Ing. degree from the University of Erlangen, Erlangen, Germany, in 1985. He has been with the Department of Electronics Engineering, University Federico Santa Maria since 1977, where he is currently full professor and rector. Now he is rector at Universidad Andres Bello. He has co-authored more than 250 journal and conference papers. His main research interests include multilevel inverters, new converter topologies, control of power converters, and adjustable-speed drives. He is associate editor of the IEEE Transactions on Power Electronics and IEEE Transactions on Industrial Electronics since 2002. He is member of the Chilean Academy of Engineering and fellow of the IEEE.